Remote Sensing of Environment 162 (2015) 154–168

Contents lists available at ScienceDirect

Remote Sensing of Environment

journal homepage: www.elsevier.com/locate/rse

Comparison of four EVI-based models for estimating gross primary production of maize and soybean croplands and tallgrass prairie under severe drought

Jinwei Dong [a,*], Xiangming Xiao [a,b,*], Pradeep Wagle [a], Geli Zhang [a], Yuting Zhou [a], Cui Jin [a], Margaret S. Torn [c], Tilden P. Meyers [d], Andrew E. Suyker [e], Junbang Wang [f], Huimin Yan [f], Chandrashekhar Biradar [g], Berrien Moore III [h]

[a] Department of Microbiology and Plant Biology, and Center for Spatial Analysis, University of Oklahoma, Norman, OK 73019, USA
[b] Institute of Biodiversity Sciences, Fudan University, Shanghai, 200433, China
[c] Atmospheric Science Department, Lawrence Berkeley National Laboratory, Berkeley, CA 94720, USA
[d] Atmospheric Turbulence and Diffusion Division, NOAA/ARL, Oak Ridge, TN 37831, USA
[e] School of Natural Resource, University of Nebraska, Lincoln, Lincoln, NE 68583, USA
[f] Institute of Geographic Sciences and Natural Resources Research, Chinese Academy of Sciences, Beijing 100101, China
[g] International Center for Agricultural Research in Dry Areas, the Consultative Group on International Agricultural Research (CGIAR), Amman, 11195, Jordan
[h] College of Atmospheric and Geographic Sciences, University of Oklahoma, Norman, OK 73019, USA

ARTICLE INFO

Article history:
Received 9 August 2014
Received in revised form 16 February 2015
Accepted 20 February 2015
Available online xxxx

Keywords:
Gross primary production (GPP)
Drought
Light use efficiency (LUE)
Vegetation Photosynthesis Model (VPM)
Temperature and Greenness (TG) model
Greenness and Radiation (GR) model
Vegetation Index (VI) model

ABSTRACT

Accurate estimation of gross primary production (GPP) is critical for understanding ecosystem response to climate variability and change. Satellite-based diagnostic models, which use satellite images and/or climate data as input, are widely used to estimate GPP. Many models used the Normalized Difference Vegetation Index (NDVI) to estimate the fraction of absorbed photosynthetically active radiation (PAR) by vegetation canopy ($FPAR_{canopy}$) and GPP. Recently, the Enhanced Vegetation Index (EVI) has been increasingly used to estimate the fraction of PAR absorbed by chlorophyll ($FPAR_{chl}$) or green leaves ($FPAR_{green}$) and to provide more accurate estimates of GPP in such models as the Vegetation Photosynthesis Model (VPM), Temperature and Greenness (TG) model, Greenness and Radiation (GR) model, and Vegetation Index (VI) model. Although these EVI-based models perform well under non-drought conditions, their performances under severe droughts are unclear. In this study, we run the four EVI-based models at three AmeriFlux sites (rainfed soybean, irrigated maize, and grassland) during drought and non-drought years to examine their sensitivities to drought. As all the four models use EVI for FPAR estimate, our hypothesis is that their different sensitivities to drought are mainly attributed to the ways they handle light use efficiency (LUE), especially water stress. The predicted GPP from these four models had a good agreement with the GPP estimated from eddy flux tower in non-drought years with root mean squared errors (RMSEs) in the order of 2.17 (VPM), 2.47 (VI), 2.85 (GR) and 3.10 g C m^{-2} day^{-1} (TG). But their performances differed in drought years, the VPM model performed best, followed by the VI, GR and TG, with the RMSEs of 1.61, 2.32, 3.16 and 3.90 g C m^{-2} day^{-1} respectively. TG and GR models overestimated seasonal sum of GPP by 20% to 61% in rainfed sites in drought years and also overestimated or underestimated GPP in the irrigated site. This difference in model performance under severe drought is attributed to the fact that the VPM uses satellite-based Land Surface Water Index (LSWI) to address the effect of water stress (deficit) on LUE and GPP, while the other three models do not have such a mechanism. This study suggests that it is essential for these models to consider the effect of water stress on GPP, in addition to using EVI to estimate FPAR, if these models are applied to estimate GPP under drought conditions.

1. Introduction

Photosynthesis of terrestrial ecosystems is a critical process in regulating carbon dioxide exchange between land and atmosphere and providing fundamental ecosystem services (food, wood, biofuel, bio-energy materials) (Beer et al., 2010). Gross primary production (GPP) from photosynthesis has been well understood at leaf and canopy levels;

* Corresponding authors at: Department of Microbiology and Plant Biology, University of Oklahoma, 101 David L. Boren Blvd., Norman, OK 73019-5300, USA.
E-mail addresses: Jinwei.dong@ou.edu (J. Dong), xiangming.xiao@ou.edu (X. Xiao).
URL's: http://www.eomf.ou.edu (J. Dong), http://www.eomf.ou.edu (X. Xiao).

http://dx.doi.org/10.1016/j.rse.2015.02.022
0034-4257/

however, ecosystem level estimation of GPP has not yet been well investigated (Asaf et al., 2013; Barman, Jain, & Liang, 2014). Since the 1990s, the eddy covariance method has been used as an important tool to measure heat, water, and CO_2 exchanges as well as trace green-house gases (Baldocchi, 2014). The observed net ecosystem CO_2 exchange (NEE) at the ecosystem scale is partitioned into GPP and ecosystem respiration (R_e, including both autotrophic and heterotrophic respiration components) (Desai et al., 2008; Papale et al., 2006; Reichstein et al., 2005). However, due to the limited number of flux tower sites and their footprints, estimation of GPP at the regional and global scales still relies on model simulation. The GPP data derived from eddy covariance flux towers (GPP_{EC}, hereafter) provides important validation data for evaluation of GPP estimates from different models.

A number of satellite-based diagnostic models use vegetation indices (VI) derived from optical sensors and climate data to estimate GPP at the site, regional, and global scales (Song, Dannenberg, & Hwang, 2013). Most of these satellite-based models, built upon the Monteith's production efficiency concept (Monteith, 1972, 1977), estimate GPP and net primary production (NPP) as a product of photosynthetic active radiation (PAR), the fraction of PAR absorbed by vegetation canopy (FPAR) and light use efficiency (ε) ($GPP = FPAR \times PAR \times \varepsilon$). These models can be divided into two groups, dependent upon their approaches to estimate absorbed PAR ($APAR = PAR \times FPAR$) (Xiao, Zhang, Hollinger, Aber, & Moore, 2005) (Fig. 1). One group models, such as the Global Production Efficiency Model (GloPEM) (Prince, 1995), Carnegie–Ames–Stanford Approach (CASA) model (Potter, 1999; Potter et al., 1993), and Photosynthesis (PSN) model (Running, Thornton, Nemani, & Glassy, 2000; Zhao, Heinsch, Nemani, & Running, 2005), use the FPAR at the canopy level ($FPAR_{canopy}$). These models often use the Normalized Difference Vegetation Index (NDVI) to estimate $FPAR_{canopy}$. Vegetation canopy is comprised of both photosynthetic (chlorophyll or green leaves) and non-photosynthetic components of vegetation. The other group models used the FPAR at the chlorophyll or green leaf level ($FPAR_{chl}$ or $FPAR_{green}$) (Gitelson et al., 2006; Sims et al., 2006; Wu, Niu, & Gao, 2010; Xiao, Zhang, et al., 2004; Zhang, Middleton, Cheng, & Landis, 2013; Zhang et al., 2006, 2009) (Fig. 1). The Vegetation Photosynthesis Model (VPM) is the first GPP model that uses $FPAR_{chl}$ (Xiao, Hollinger, et al., 2004; Xiao, Zhang, et al., 2004) and the Enhanced Vegetation Index (EVI) (Huete et al., 2002) was used to estimate $FPAR_{chl}$ in VPM. Gitelson, Peng, Arkebauer and Schepers (2014), Gitelson, Vina, Ciganda, Rundquist and Arkebauer (2005), Gitelson et al. (2006) proposed the concept of the fraction of absorbed PAR by green leaves ($FPAR_{green}$) in crops. The Vegetation Index (VI) model (Wu, Niu, & Gao, 2010) used EVI as proxies of both LUE and $FPAR_{green}$ which simplified the model structure. Several other models also used EVI to estimate GPP directly through a statistical modeling approach (Sims et al., 2008; Wu, Chen, & Huang, 2011), including the Temperature and Greenness (TG) model (Sims et al., 2006, 2008) and the Greenness and Radiation (GR) model (Gitelson et al., 2006) which considered EVI as the proxies of $FPAR_{green}$ and $FPAR_{chl}$, respectively. As these four models use EVI to estimate FPAR, they are referred as EVI-based model thereafter.

To better understand the global carbon-cycle feedback to climate change, it is critical to estimate GPP variability due to climate variation (e.g., drought), as it dominates the global GPP anomalies (Barman et al., 2014; Zscheischler et al., 2014). Previous studies have shown that EVI-based VPM, TG, GR, and VI models perform well in forest, grassland and cropland ecosystems under non-drought condition (Gitelson et al., 2006; Kalfas, Xiao, Vanegas, Verma, & Suyker, 2011; Sims et al., 2008; Wu, Gonsamo, Zhang, & Chen, 2014; Wu, Munger, Niu, & Kuang, 2010; Wu et al., 2011; Xiao et al., 2005). The performances of these models in agricultural and grassland ecosystems under drought conditions are still unclear (Mu et al., 2007; Schaefer et al., 2012). Drought affects (1) light absorption through changes in leaf chlorophyll content and leaf area index, and (2) LUE through increased water and

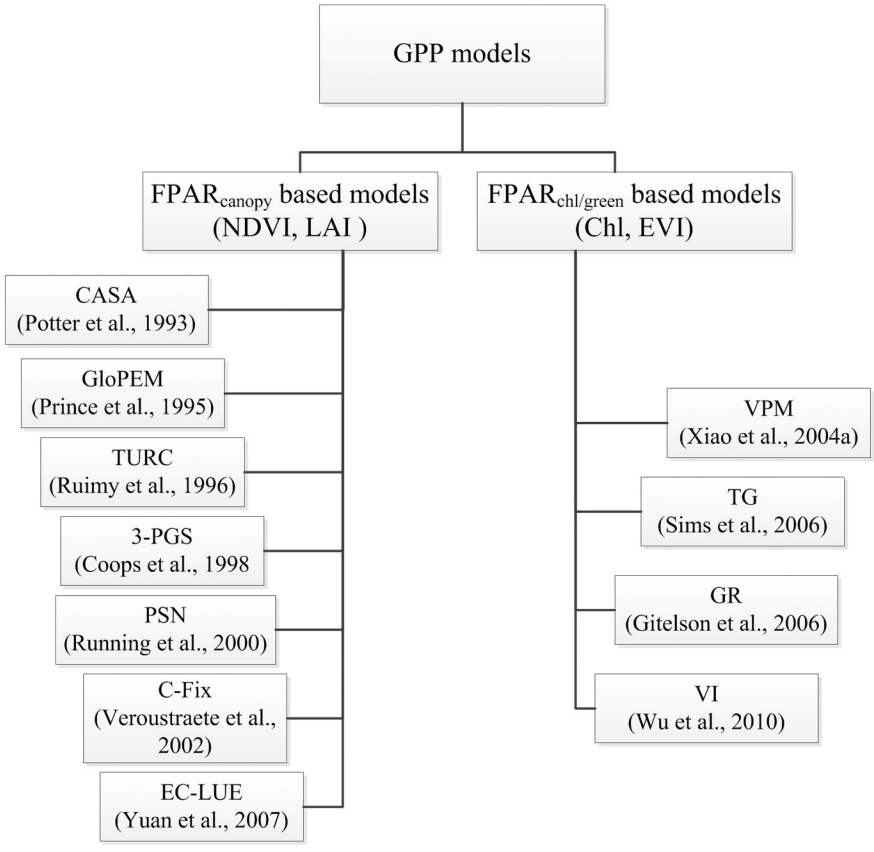

Fig. 1. Evolution of Gross Primary Production (GPP) models distinguished by the fraction of absorbed photosynthetically active radiation (FPAR).

temperature stresses, which may result in a decrease of GPP. These four EVI-based models evaluate the effect of drought on light absorption ($FPAR_{green}$ or $FPAR_{chl}$) in the same way through the use of EVI. They differ substantially in their ways to evaluate the effect of drought on LUE. Specifically, no specific water stress related variables are directly considered in the TG, GR, and VI models (Gitelson et al., 2006; Sims et al., 2008; Wu, Niu, & Gao, 2010). For example, in the TG model, water stress was considered by transferring land surface temperature (LST) as an alternative approach (Sims et al., 2006, 2008). The VI model uses EVI as proxy of a synthetic LUE (Wu, Munger, et al., 2010). In the VPM model, LUE includes down-regulation scalars for both temperature and water stresses. The Land Surface Water Index (LSWI), which is calculated as a normalized ratio of near infrared and shortwave infrared bands, is used to estimate the effect of water stress, while air temperature is used to estimate the effect of temperature stress (Jin et al., 2013; Xiao, Hollinger, et al., 2004; Xiao, Zhang, et al., 2004). A recent study modified the water stress variable in VPM, which in turn improved the model performance in estimating GPP of grasslands under drought conditions (Wagle et al., 2014).

The objective of this study was to evaluate the performance of these four EVI-based GPP models under drought and non-drought conditions (as references) from the perspective of the model structures. Three AmeriFlux sites, including one rainfed soybean site, one prairie site, and one irrigated maize site (11 site–years), were selected for the comparison. Vegetation indices and LST products were derived from eight-day Moderate Resolution Imaging Spectroradiometer (MODIS) composite images, and climate variables were acquired from the flux tower sites. The results from this study will likely contribute to the improvement of GPP models and better understanding of GPP response to short-term climate variability, specifically severe drought.

2. Materials and methods

2.1. The CO_2 flux tower sites

2.1.1. Bondville site (US-Bo1)

This site is located in Champaign, Illinois, USA (40.0062°N, 88.2904°W, 217 m asl, Table 1). It is rainfed and no-till cropland with an annual rotation between maize and soybean (maize in the odd years and soybean in the even years since 1996). Detailed information on the site can be found in an earlier study (Meyers & Hollinger, 2004).

2.1.2. Mead irrigated site (US-Ne1)

The US-Ne1 site (41.1651°N, 96.4766°W, 355 m asl, Table 1) is located in a field at the University of Nebraska Agricultural Research and Development Center near Mead, Nebraska. This site has a center pivot system for irrigation and has been cultivated with maize crop and no-till practice. Detailed information about this site can be found in an earlier study (Suyker et al., 2005).

2.1.3. ARM Southern Great Plains burn site (US-ARb)

The US-ARb site is located in the native tallgrass prairies of the United States Department of Agriculture Grazinglands Research Laboratory (USDA-GRL), El Reno, Oklahoma, USA (35.5497°N, 98.0402°W, 423 m asl, Table 1). Dominant species are big bluestem (*Andropogon gerardi* Vitman), little bluestem (*Schizachyrium halapense* (Michx.) Nash.), and other grasses common to tallgrass prairie. The plot was burned on March 8, 2005. Detailed information on the site can be found in an earlier study (Fischer et al., 2012).

2.2. Data

2.2.1. CO_2 eddy flux and meteorological data

The AmeriFlux website (http://ameriflux.lbl.gov/) provides datasets of carbon, water and energy fluxes, and meteorological variables for individual flux tower sites (Agarwal et al., 2010). Eleven site–years of data were acquired from the AmeriFlux website, including three years of data (2002, 2004, and 2006) for the US-Bo1 site, two years of data (2005–2006) for the US-ARb site, and six years of data (2007–2012) for the US-Ne1 site. Level 4 eight-day data were used in this study to match the temporal resolution of the MODIS 8-day surface reflectance composite datasets. We used the gap-filled and partitioned GPP data from the Marginal Distribution Sampling (MDS) method (Reichstein et al., 2005). The meteorological data used in this study include air temperature, precipitation, vapor pressure deficit (VPD), and solar radiation. Solar radiation was converted to photosynthetically active radiation (PAR, mol PPFD).

2.2.2. MODIS surface reflectance, vegetation index and land surface temperature data

The MODIS 8-day surface reflectance composite data (MOD09A1) during 2000–2012 for individual flux tower sites were downloaded from the data portal at the University of Oklahoma (http://www.eomf.ou.edu/visualization/). We calculated three vegetation indices, including EVI (Huete, Liu, Batchily, & vanLeeuwen, 1997; Huete et al., 2002), NDVI (Tucker, 1979), and LSWI (Xiao, Zhang, et al., 2004; Xiao et al., 2005), using the reflectance data as shown below:

$$\mathrm{NDVI} = \frac{\rho_{\mathrm{NIR}} - \rho_{\mathrm{Red}}}{\rho_{\mathrm{NIR}} + \rho_{\mathrm{Red}}} \quad (1)$$

$$\mathrm{EVI} = 2.5 \times \frac{\rho_{\mathrm{NIR}} - \rho_{\mathrm{Red}}}{\rho_{\mathrm{NIR}} + 6 \times \rho_{\mathrm{Red}} - 7.5 \times \rho_{\mathrm{Blue}} + 1} \quad (2)$$

$$\mathrm{LSWI} = \frac{\rho_{\mathrm{NIR}} - \rho_{\mathrm{SWIR}}}{\rho_{\mathrm{NIR}} + \rho_{\mathrm{SWIR}}} \quad (3)$$

where ρ_{Blue}, ρ_{Red}, ρ_{NIR}, and ρ_{SWIR} are the surface reflectance values of blue (459–479 nm), red (620–670 nm), near infrared (841–875 nm), and shortwave infrared (SWIR: 1628–1652 nm).

The MODIS 8-day land surface temperature and emissivity products (MOD11A2) during 2000–2012 were also downloaded from the data portal at the University of Oklahoma. The MOD11A2 data have both daytime (10:30 am) and nighttime (10:30 pm) land surface temperature (LST). The daytime LST DN values were converted to temperature (°C unit) using the equation, $LST = DN \times 0.02 - 273.15$. Both MOD09A1 and MOD11A2 datasets provide data quality flags. For those observations with the bad quality flags (e.g., clouds and cloud shadows), the linear interpolation method was used for gap-filling time series data within a year (Meijering, 2002).

Table 1
Brief description of the CO_2 eddy flux tower sites used in this study.

Site ID	Site name	Site location	Years	Vegetation	References
US-Bo1	Bondville	40.0062°N, 88.2904°W	2002[a], 2004, 2006	Soybean	Meyers and Hollinger (2004)
US-Ne1	Mead-irrigated continuous maize site	41.1650°N, 96.4766°W	2007, 2008, 2009, 2010, 2011, 2012[a]	Maize	Suyker, Verma, Burba, and Arkebauer (2005)
US-ARb	ARM Southern Great Plains Burnt site	35.5497°N, 98.0402°W	2005, 2006[a]	Tallgrass prairie (bluestem)	Fischer et al. (2012)

[a] Drought years, based on vapor pressure deficit (VPD) and other indicators including precipitation and temperature.

The GPP estimates from the MODIS standard GPP products (both MOD17A2 Version-5 and Version-55) were also downloaded and used for comparison with the GPP estimates of the four EVI-based models. The MOD17A2 products were generated by the Numerical Terradynamic Simulation Group (NTSG), University of Montana (UMT), and detailed algorithms are available in the previous publications (Running et al., 2004; Zhao & Running, 2010; Zhao et al., 2005). The difference in these two versions is that the new version (V55) used a consistent forcing meteorology and considered the cloud-contamination issue while the older version (V5) did not, thus the MOD17A2-V55 products can avoid the underestimations in the MOD17A2-V5 products (Sjöström et al., 2011; Zhao & Running, 2010).

2.3. The EVI-based GPP models

Here we provide a brief description of the four EVI-based GPP models used in this study (Table 2). Detailed descriptions of these models can be found in previous publications (Gitelson et al., 2006; Sims et al., 2006, 2008; Wagle et al., 2014; Wu, Munger, et al., 2010; Wu, Niu, & Gao, 2010; Wu, Gonsamo, Zhang, et al., 2014; Xiao, Zhang et al., 2004).

2.3.1. The vegetation photosynthesis model (VPM)

The VPM model estimates GPP as the product of PAR, $FPAR_{chl}$, and LUE,

$$GPP_{VPM} = \varepsilon_g \times FPAR_{chl} \times PAR \quad (4)$$

where ε_g is the light use efficiency (g C mol^{-1} photosynthetic photon flux density, PPFD), $FPAR_{chl}$ is the fraction of PAR absorbed by chlorophyll, and PAR is the photosynthetically active radiation.

The $FPAR_{chl}$ is estimated as a linear function of EVI,

$$FPAR_{chl} = a \times EVI \quad (5)$$

where the coefficient a is set to be 1.0 (Xiao, Zhang, et al., 2004).

The light use efficiency ε_g is derived by down-regulating the maximum LUE (ε_0) with scalars of temperature and water stresses.

$$\varepsilon_g = \varepsilon_0 \times T_{scalar} \times W_{scalar} \quad (6)$$

where ε_0 is the apparent quantum yield or maximum light use efficiency (g C mol^{-1} PPFD), which is usually determined using the Michaelis–Menten function based on NEE and PPFD data at 30-minute intervals during peak growth at the eddy flux sites (Goulden et al., 1997). Based on previous publications, we used the ε_0 value of 0.39 g C mol^{-1} PPFD at the US-Bo1 site (soybean), 0.42 g C mol^{-1} PPFD at the US-ARb site (tallgrass prairie), and 0.69 g C mol^{-1} PPFD at the US-Ne1 site (corn) (Kalfas et al., 2011; Wagle, Xiao, & Suyker, 2015; Wagle et al., 2014).

T_{scalar} is estimated at each time step as in the Terrestrial Ecosystem Model (Raich et al., 1991),

$$T_{scalar} = \frac{(T-T_{min})(T-T_{max})}{(T-T_{min})(T-T_{max}) - \left(T-T_{opt}\right)^2} \quad (7)$$

where T_{min}, T_{max}, and T_{opt} represent minimum, maximum, and optimum temperatures for photosynthetic activities, respectively. In this study, we set T_{min}, T_{opt}, and T_{max} values to −1 °C, 30 °C, and 50 °C, respectively, at the US-Bo1 (soybean, Wagle et al., 2015) and US-ARb (tallgrass prairie, Wagle et al., 2014) sites, and to 10 °C, 28 °C, and 48 °C at the US-Ne1 (corn, Kalfas et al., 2011) site.

W_{scalar} is estimated at each time step based on the MODIS-based LSWI. A two-step W_{scalar} function was implemented to address the effect of water stress (Wagle et al., 2014, 2015).

$$W_{scalar} = \begin{cases} \dfrac{1+LSWI}{1+LSWI_{max}} & (LSWI > 0) \\ LSWI_0 + LSWI & (LSWI \le 0) \end{cases} \quad (8)$$

where $LSWI_{max}$ is the maximum LSWI within the growing season and $LSWI_0$ is the average of maximum LSWI values in the growing season cycles over multiple years.

2.3.2. The temperature and greenness (TG) model

The TG model estimates GPP as a product of scaled canopy greenness (i.e., EVI) and scaled LST (Sims et al., 2008).

$$GPP_{TG} = (scaledLST \times scaledEVI) \times m \quad (9)$$

where *ScaledLST* is determined according to the relationship between LST and GPP, and two linear equations are used to define it. This design accounts for the drought conditions with high temperature and high VPD stress (Sims et al., 2008). m is a scalar with the unit of mol C m^{-2} day^{-1} and was determined based on the model calibration stated in the following section.

$$scaledLST = \min\left(\frac{LST}{30}, 2.5-0.05 \times LST\right) \quad (10)$$

ScaledEVI is estimated by subtracting 0.1 from EVI as GPP drops to zero when EVI reaches 0.1 (Sims et al., 2006).

$$scaledEVI = EVI-0.1 \quad (11)$$

2.3.3. The greenness and radiation (GR) model

The GR model estimates GPP by using crop chlorophyll content and incoming solar radiation. The model has been used in irrigated and rainfed maize croplands (Gitelson et al., 2006; Peng, Gitelson, Keydan, Rundquist, & Moses, 2011), wheat croplands (Wu et al., 2009), and forests (Wu, Gonsamo, Gough, Chen, & Xu, 2014).

$$GPP = PAR \times Chl \times m \quad (12)$$

Recently, EVI was used to replace the Chlorophyll content in the model (Wu, Niu, Wang, Gao, & Huang, 2010). m is a scalar with the unit of mol C m^{-2} day^{-1}, and was determined based on the model calibration as described in the following section (Section 2.4).

2.3.4. The vegetation index (VI) model

The VI model (Wu, Niu, & Gao, 2010) estimates GPP using EVI and PAR data, and also assumes that EVI is related to photosynthesis capacity (Gitelson et al., 2006; Wu et al., 2009). The model has been used in maize and deciduous forest and proven to work reasonably well (Wu et al., 2009; Wu, Niu, & Gao, 2010).

$$GPP = PAR \times EVI \times EVI \times m \quad (13)$$

where m is a scalar with the unit of mol C m^{-2} day^{-1} and was determined based on the model calibration described in the following section (Section 2.4).

2.4. Calibration of TG, VI, and GR models

Model calibration has a large impact on model accuracy (Yuan et al., 2007). The TG, VI, and GR models need calibration to estimate the value of parameter m. The usual approach for model calibration is to use part of the available data (Peng et al., 2011; Sims et al., 2008; Wu et al., 2012). Some previous studies used all the samples in calibration of the models (Wu, Gonsamo, Zhang, et al., 2014). In this model comparison study, for the purpose of simplification and given the small volume of available data, we used the GPP data from all the years to calibrate the models at the individual sites. Specifically, for each site we used all the GPP_{EC} data in the growing season to empirically estimate the m values for the TG, VI and GR models, which was likely to result in exceeding normal performances of the TG, VI, and GR models.

Table 2
The model structures and parameters of the four EVI-based models that estimate gross primary production (GPP) of vegetation.

Model	PAR	FPAR concept	FPAR estimation	LUE (ε_g) or environmental down-regulating	References
VPM	PAR	$FPAR_{chl}$	f(EVI)	$\varepsilon_0 \times T_{scalar} \times W_{scalar}$	Wagle et al. (2014) and Xiao et al. (2004b)
GR	PAR	$FPAR_{chl}$	f(EVI)	–	Gitelson et al. (2006) and Wu, Gonsamo, Zhang, et al. (2014)
TG	–	$FPAR_{green}$	f(EVI)	f(LST)	Sims et al. (2006, 2008)
VI	PAR	$FPAR_{green}$	f(EVI)	f(EVI)	Wu, Munger, et al. (2010) and Wu, Niu, and Gao, 2010 (2010)

In comparison, the VPM model does not need a calibration process for the flux tower sites used in this study. It uses parameter values from previous publications, such as maximum LUE parameters (Kalfas et al., 2011; Wagle et al., 2014, 2015). It also uses parameter values from a standardized parameterization procedure, for example, T_{scalar} and W_{scalar} in the model.

2.5. Evaluation of model performance

The predicted GPPs from the four models (GPP_{VPM}, GPP_{TG}, GPP_{VI}, and GPP_{GR}) were evaluated against the GPP_{EC}. First, the seasonal dynamics of the simulated GPPs were compared. Second, the Pearson's correlation coefficient (r) and the root mean squared error (RMSE) were calculated

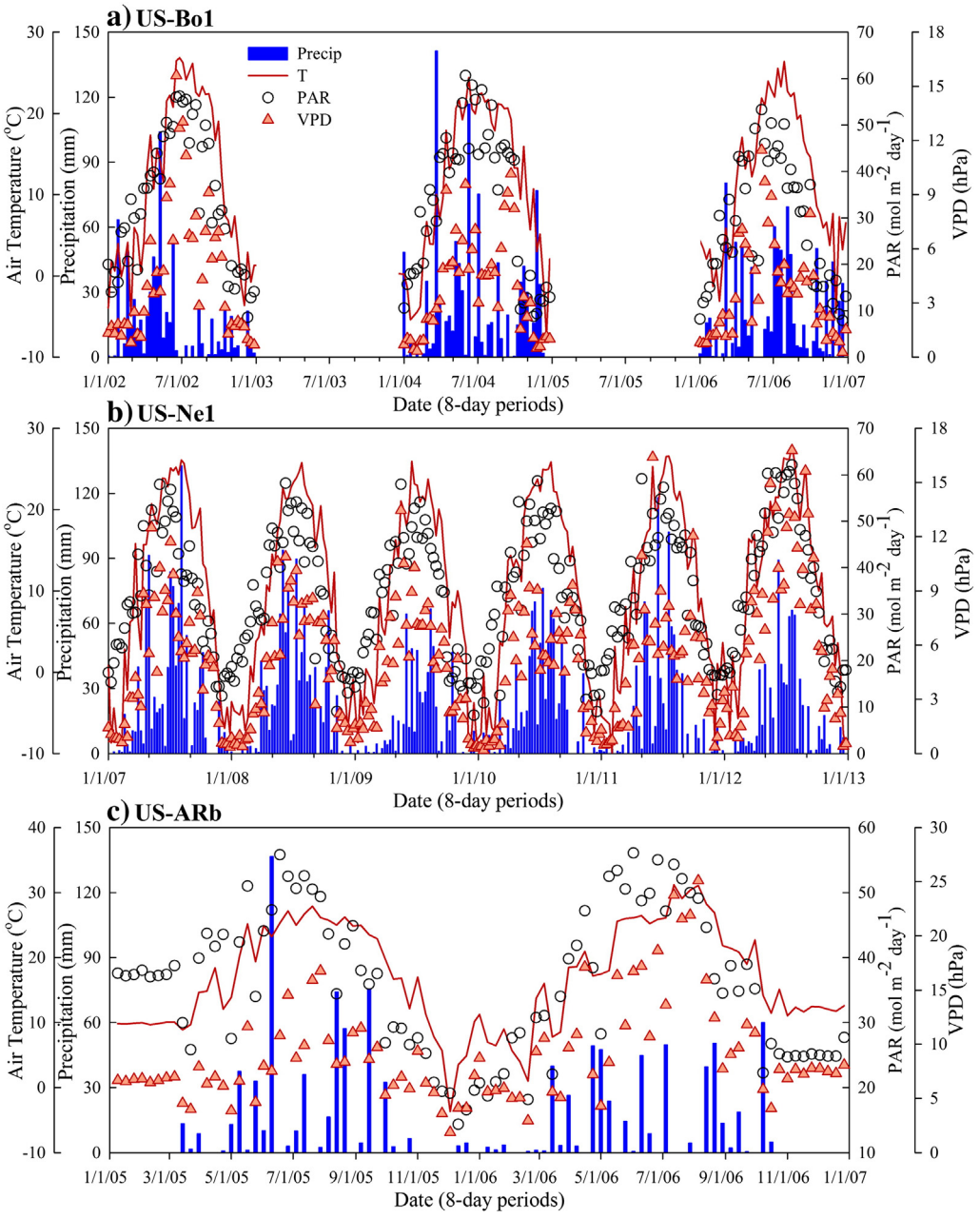

Fig. 2. Seasonal dynamics and interannual variations of air temperature, precipitation, photosynthetically active radiation (PAR), and vapor pressure deficit (VPD) with an interval of 8-days at the three flux tower sites (a. US-Bo1, b. US-Ne1, and c. US-ARb).

Table 3
Meteorological statistics in the growing seasons of different site–years to identify droughts.

Site ID	Years	VPD_{mean} (hPa)	Precipitation (mm)	Ta_f_{mean} (°C)	Rg_f_{mean} ($MJ\ m^{-2}\ day^{-1}$)
US-Bo1	2002[a]	8.49	153	23.54	22.37
	2004	5.48	367	20.96	22.68
	2006	5.86	362	22.15	19.41
	Average	6.61	294	22.22	21.49
US-Ne1	2007	7.53	605	22.49	20.72
	2008	7.83	690	21.02	20.42
	2009	7.56	457	20.56	20.94
	2010	6.78	634	22.82	22.38
	2011	7.22	515	20.92	20.99
	2012[a]	12.01	514	23.16	24.84
	Average	8.12	569	21.76	21.64
US-ARb	2005	8.99	546	22.27	19.41
	2006[a]	13.42	432	23.47	20.16
	Average	11.16	489	22.86	19.78

[a] Drought years.

to quantify the agreement between GPP_{EC} and predicted GPPs during the plant growing season. In addition, the linear regression model was used to determine the relationship between predicted GPPs and GPP_{EC}, and the coefficient of determination (R^2) was used to evaluate the models' explanatory abilities for GPP variances. Third, the seasonally integrated GPPs can quantify biases of the modeled GPPs in magnitude.

3. Results

3.1. Comparison of climate, GPP, and vegetation indices in drought and non-drought years

We identified site–years that experienced severe droughts during the plant growing season based on meteorological data. Following the same definition as in previous works (Jin et al., 2013; Kalfas et al., 2011; Wagle et al., 2014), the plant growing season was defined as the period of GPP > 1 g C m^{-2} day^{-1}. The US-Bo1, US-Ne1, and US-

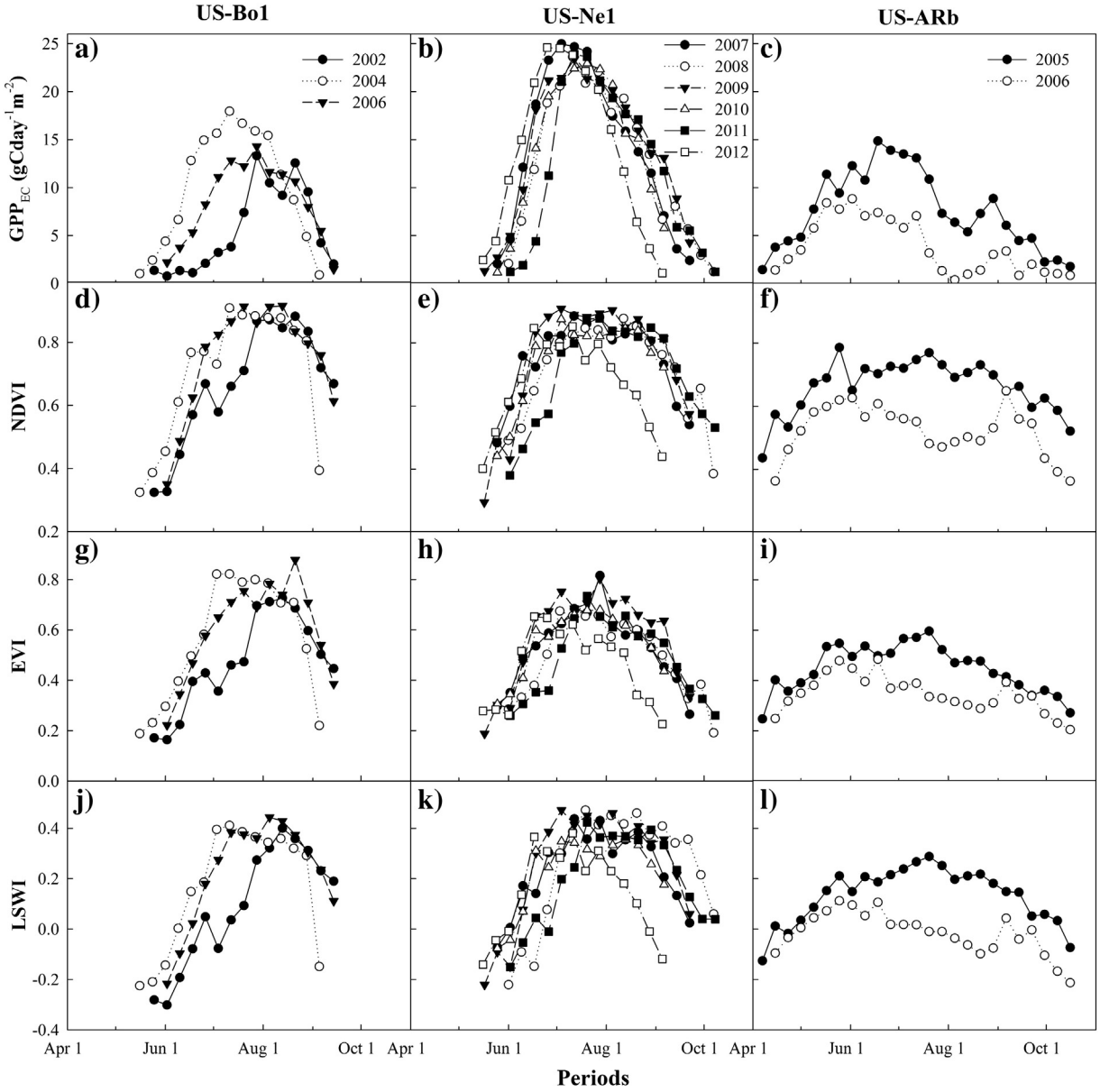

Fig. 3. Seasonal dynamics and interannual variations of gross primary production (GPP_{EC}) (a. US-Bo1, b. US-Ne1, and c. US-ARb) and vegetation indices at the three CO_2 flux sites, including NDVI (d. US-Bo1, e. US-Ne1, and f. US-ARb), EVI (g. US-Bo1, h. US-Ne1, and i. US-ARb), and LSWI(j. US-Bo1, k. US-Ne1, and l. US-ARb).

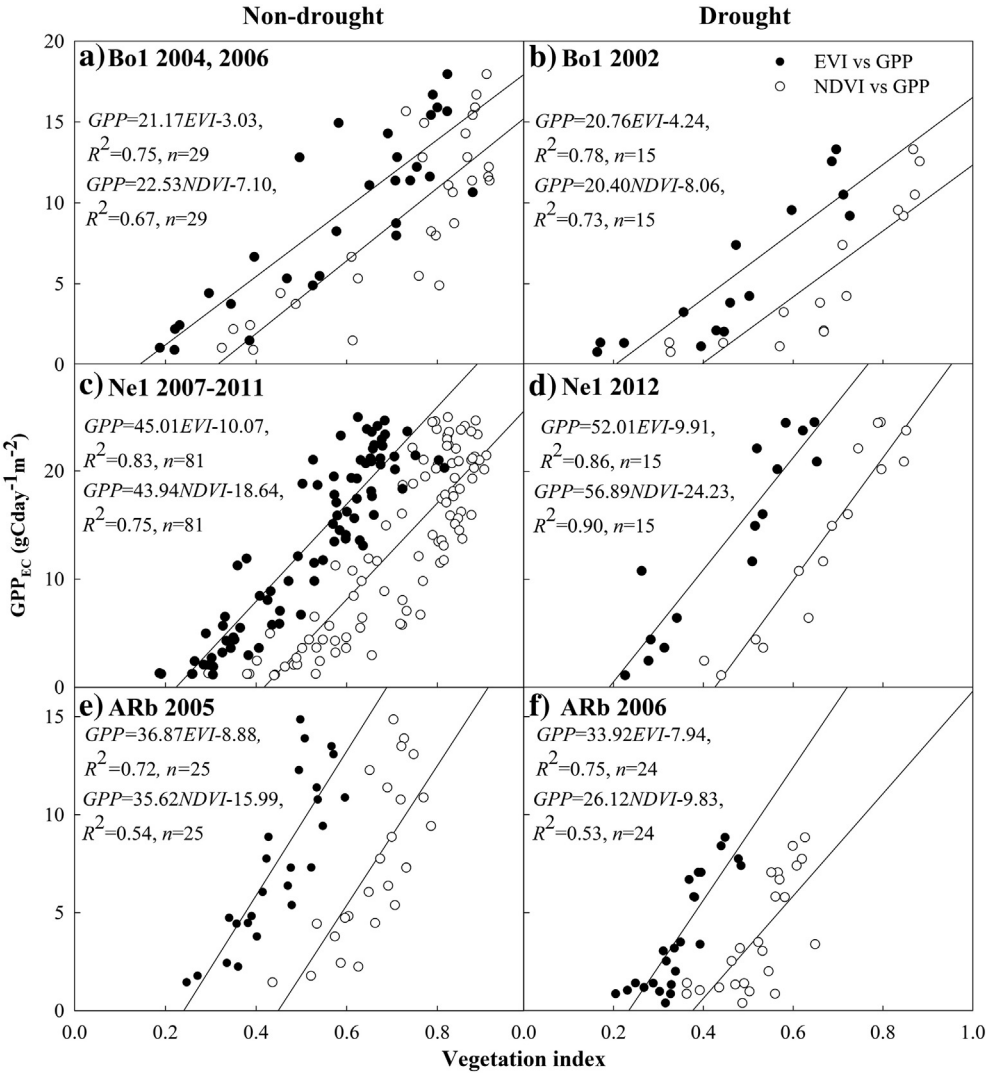

Fig. 4. The relationships between gross primary production (GPP_{EC}) and vegetation indices (NDVI and EVI) in the drought years (a. US-Bo1 2004, 2006; c. US-Ne1 2007–2011; and e. US-ARb 2005) and non-drought years (b. US-Bo1 2002, d. US-Ne1 2012, and f. US-ARb 2006) at the three CO2 flux tower sties.

ARb sites showed drought signals in 2002, 2012, and 2006, respectively, as indicated by VPD (Fig. 2, Table 3). The US-Bo1 site had an average VPD of 8.49 hPa in the 2002 growing season, much higher than in 2004 (5.48 hPa) and 2006 (5.86 hPa). Also, its precipitation in the 2002 growing season was 153 mm, which was at least 50% lower than other years (367 mm in 2004 and 362 mm in 2006, Table 3). The US-Ne1 site experienced drought in 2012 with a high VPD of 12.01 hPa while the average VPD in 2007–2011 was only 7.40 hPa (Table 3). At the US-ARb site, the VPD in the 2006 growing season was 49% higher than in 2005, also the precipitation in 2006 was 21% less than in 2005. All three sites also had higher air temperature and radiation in the drought years than in non-drought years (Fig. 2).

Observed carbon fluxes and satellite-based vegetation indices dropped significantly in those drought years, i.e., 2002 at US-Bo1, 2012 at US-Ne1 and 2006 at US-ARb (Fig. 3). At the US-Bo1 site, the average GPP_{EC} of soybean in the 2002 growing season decreased by 40% relative to the non-drought years (2004 and 2006), while NDVI, EVI and LSWI decreased by 9%, 19%, and 55%, respectively. The same phenomenon also happened at the US-ARb site; the average GPP_{EC} of grassland in the 2006 growing season decreased by 49% compared to those of the non-drought years (2005), while NDVI, EVI, and LSWI decreased by 21%, 22%, and 111%, respectively. At the irrigated US-Ne1 site, GPP_{EC} dropped significantly in August, as did NDVI, EVI and LSWI (Fig. 3).

3.2. The relationships between vegetation indices (NDVI and EVI) and GPP_{EC} in drought and non-drought years

We regrouped all data into (1) non-drought years and (2) drought years for each site, and carried out simple linear regression analysis of GPP_{EC} and vegetation indices (NDVI and EVI). For the non-drought site-years, EVI accounted for more variance of GPP (with higher coefficient of determination) than did NDVI (Fig. 4a, c, and e). For example, at the US-Bo1 site in 2004 and 2006, the EVI and NDVI accounted for 75% and 67% of GPP variances, respectively. For the drought site–years, EVI also accounted for more GPP variance than did NDVI. At the US-Bo1 site in 2002, the EVI and NDVI accounted for 78% and 73% of GPP variances, respectively (Fig. 4b). At the US-ARb site in 2006, EVI and NDVI explained 75% and 53% of GPP variances (Fig. 4f). At the US-Ne1 site in 2012, EVI and NDVI accounted similarly for GPP variances, at 86% and 90%, respectively (Fig. 4d). In general, EVI better explained GPP variances than did NDVI under both non-drought and drought conditions.

For comparison between the drought and non-drought site–years, the results showed that the linear relationship between vegetation indices (EVI and NDVI) and GPP_{EC} was slightly stronger during the drought site–years (Fig. 4b, d, and f) than the non-drought site–years (Fig. 4a, c, and e). This demonstrated that the sensitivity of EVI and NDVI to GPP

could be higher under drought (water stress) than non-drought conditions. However, to confirm this result, additional data analysis in drought and non-drought years is still needed in the future.

3.3. Comparison of GPP estimates from the models (VPM, TG, GR, and VI) and flux towers in drought and non-drought years

3.3.1. Seasonal dynamics of GPP estimates from models and towers

Fig. 5 shows that the seasonal dynamics of GPP estimates from the four EVI-based models tracked GPP_{EC} reasonably well during drought and non-drought years at all three study sites, despite the difference in growing season lengths and water management (irrigation and rainfed). The growing season of soybean at the US-Bo1 site starts between May 16 and June 2 and ends between September 5 and 14 (Table 4). Corn crops at the US-Ne1 site had similar starting dates but a longer growing season that lasted till early October. Grassland in the US-ARb site had the longest growing season, from early April to mid-October (Fig. 3). As drought occurred on different dates and lasted for various lengths of time, the effects of drought on seasonal dynamics of GPP and vegetation indices were different at each site. At the US-Bo1 site (2002), drought first occurred in late June and lasted until late July. At the US-Ne1 site, drought began in late July and lasted until early September. The drought at the US-Ne1 site led to an earlier harvest of corn crops in 2012 in comparison to other years (2007–2011). The drought at the US-ARb site (2006) started from early June to September. In general, all four models captured the seasonal dynamics very well in non-drought years and fairly well in drought years.

Besides the starting and end dates of the growing season, we also compared the emergence dates when the maximum GPP appeared (Table 4). RMSEs of GPP_{EC} and GPP_{VPM} as well as GPP_{TG} had a lowest deviation of 15 days while GPP_{VI} and GPP_{GR} had a larger deviation with GPP_{EC} (18 days). This indicated that VPM and TG models performed better in simulating the dates when GPP reached maximum.

3.3.2. Correlation analysis of GPP estimates from models and towers

In terms of the individual sites, the linear regression analysis indicated that in non-drought years all four models had generally good explanatory capabilities for GPP variance at the three sites (VPM: RMSE 1.87 ~ 2.27, $R^2 > 0.95$; TG: RMSE 2.58 ~ 3.35, $R^2 > 0.91$, VI: RMSE 1.84 ~ 2.68, $R^2 > 0.96$, and GR: RMSE 2.05 ~ 3.24, $R^2 > 0.95$, Fig. 6). RMSE of GPP_{EC} and GPP_{VPM} was lowest for most site–years among the four models (Table 5). The performance of the models in drought conditions was also evaluated at the individual sites (US-Bo1 2002, US-Ne1 2012, and US-ARb 2006) (Fig. 7). Results show that the four models performed differently. The VPM model had the lowest RMSE (0.99 ~ 2.39) and highest explanatory capability for GPP variance with R^2 of 0.96–0.98. GPP_{VI} also had a significant relationship with observed GPP at all three sites but with a higher RMSE (1.39 ~ 3.24) and lower explanatory capability (with R^2 of 0.94, 0.97, and 0.93 at US-Bo1, US-Ne1, and US-ARb respectively). The TG (with R^2 0.74–0.91) and GR models (with R^2 0.85–0.96) had weaker explanatory capabilities for GPP variances than the other two models during the drought years (Fig. 7). RMSE and R^2 analysis of GPP_{EC} and estimated GPP from the four models showed that VPM-based results were the most consistent with GPP_{EC} and explained the GPP variances most (Table 5).

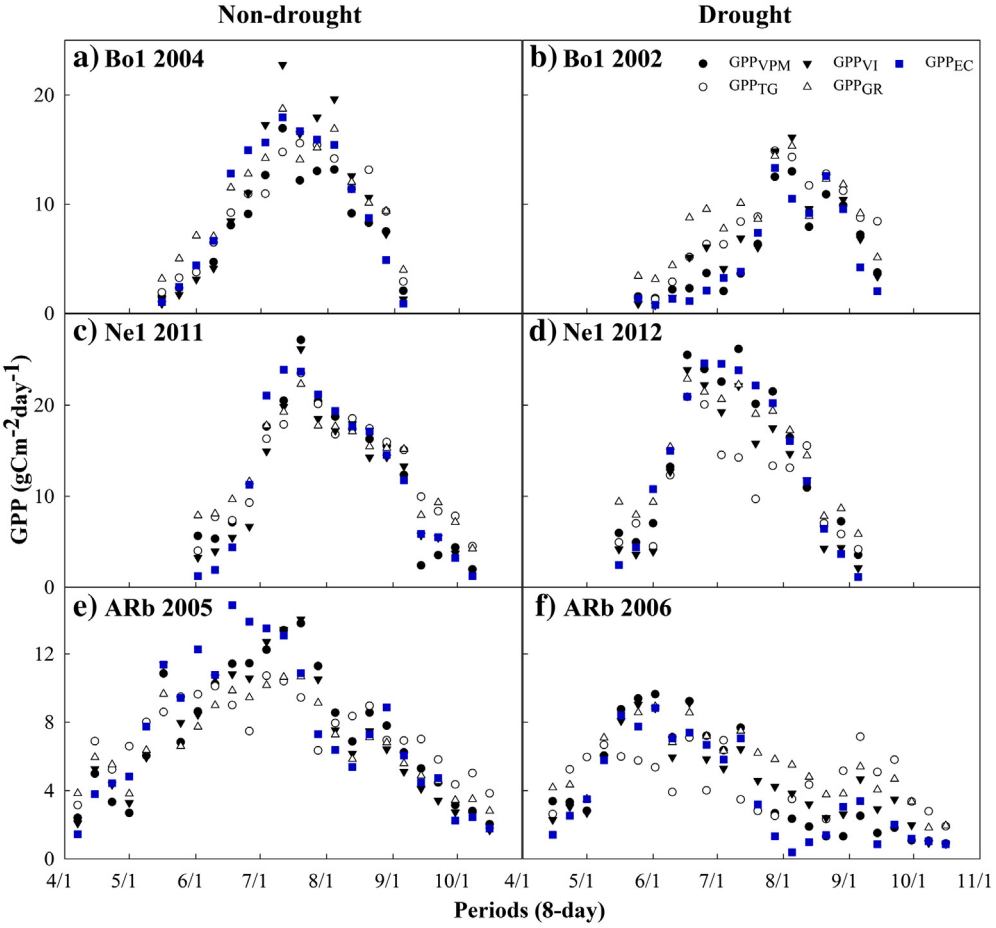

Fig. 5. A comparison on seasonal dynamics of gross primary production from the flux tower sites (GPP_{EC}) and the four EVI-based models (GPP_{VPM}, GPP_{VPM}, GPP_{VPM}, and GPP_{VPM}) in a drought year (a. US-Bo1 2004; c. US-Ne1 2011, and e. US-ARb 2005) and a non-drought year (b. US-Bo1 2002; d. US-Ne1 2012; and f. US-ARb 2006) at the three flux tower sites. To enhance the visualization, only one year of data from non-drought years was used to showcase intra-annual variation of GPPs.

Table 4
The root mean squared errors (RMSEs) between the dates of maximum GPP_{EC} and modeled GPPs for the three study sites. The growing season is defined as the period with GPP > 1 g C m^{-2} day^{-1}.

Site	Year	Growing season	GPP_{EC}	GPP_{VPM}	GPP_{TG}	GPP_{VI}	GPP_{GR}
US-Bo1	2002[a]	5/25–9/14	7/28	8/5	7/28	8/5	8/5
	2004	5/16–9/5	7/11	8/4	7/19	8/4	8/4
	2006	6/2–9/14	7/28	7/28	7/12	8/21	8/21
US-Ne1	2007	5/25–9/22	7/4	7/12	7/28	7/28	7/28
	2008	6/1–10/7	7/11	7/27	7/27	7/27	7/27
	2009	5/17–9/22	7/12	7/4	7/28	7/28	7/28
	2010	5/25–9/6	7/20	7/12	8/5	7/28	7/28
	2011	6/2–10/8	7/12	7/20	7/20	7/20	7/20
	2012[a]	5/16–9/5	6/25	7/11	6/17	6/25	6/17
US-ARb	2005	4/7–10/16	6/18	7/20	7/4	7/20	7/20
	2006[a]	4/15–10/16	6/2	6/2	6/18	6/18	6/2
RMSEs of peak GPP dates				15d	15d	18d	18d

[a] Drought years.

In terms of all the non-drought site–years, Fig. 8 shows that simulated GPP from all four models (GPP_{VPM}, GPP_{TG}, GPP_{VI} and GPP_{GR}) had reasonably good agreement with GPP_{EC} ($R^2 > 0.95$). That being said, in each drought site–year, the four models had different performances. The GPP_{VPM} was significantly correlated with GPP_{EC} ($R^2 = 0.97$, Fig. 8). The VI model also had a significant relationship with GPP_{EC} but with slightly lower explanatory capability ($R^2 = 0.94$), while TG and GR models had lower explanation of GPP_{EC} variances (TG, $R^2 = 0.84$; GR, $R^2 = 0.91$) in terms of all the drought site–years (Fig. 8). RMSE of GPP_{EC} and GPP_{VPM} was the lowest (1.61 g C m^{-2} day^{-1}) compared to other models (TG 3.90, VI 2.32, and GR 3.16 g C m^{-2} day^{-1}).

3.3.3. Comparison of annual (seasonal) sum of GPP estimates from models and towers

The seasonally integrated GPP analysis indicated that in the non-drought site–years GPP estimates from all four models were reasonably

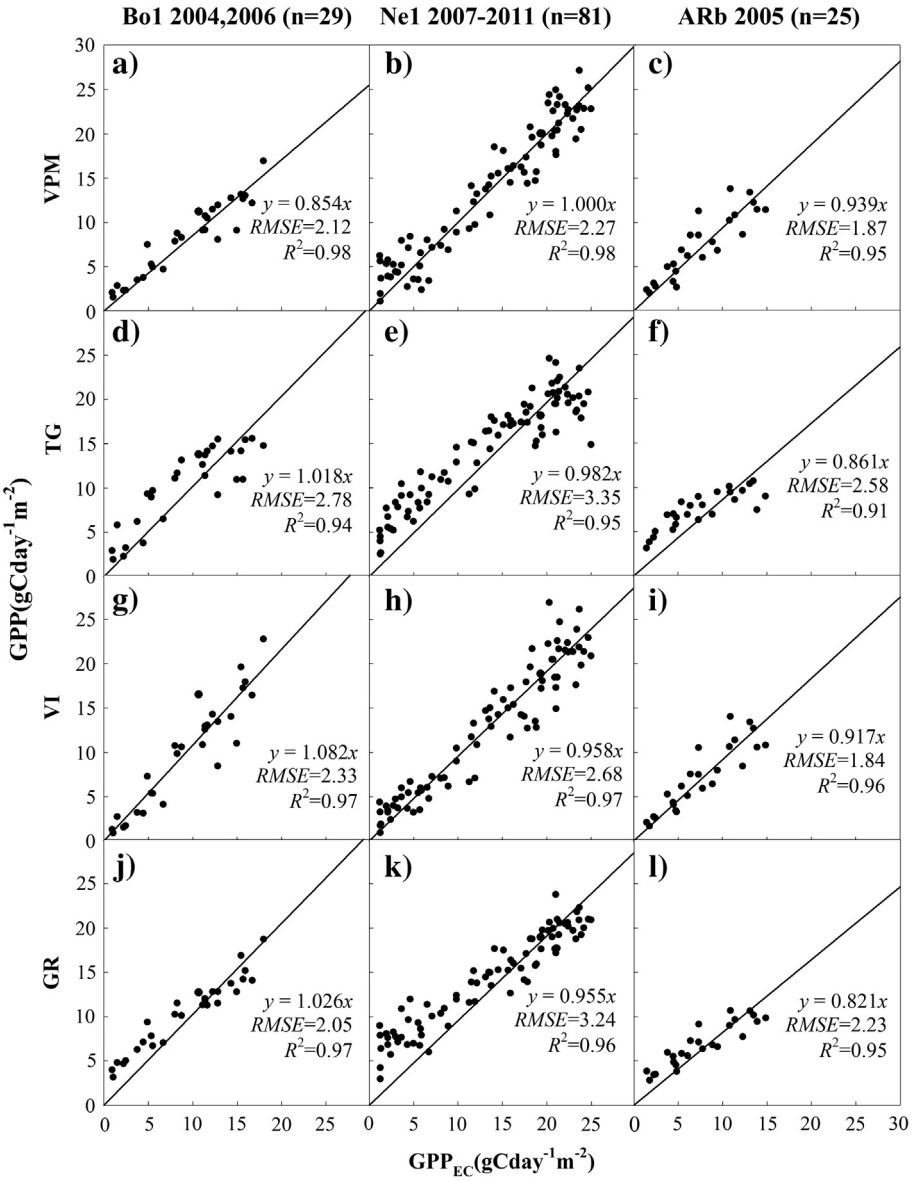

Fig. 6. The relationships between gross primary production from the CO_2 flux tower sites (GPP_{EC}) and predicted GPPs from the four models (GPP_{VPM}, GPP_{TG}, GPP_{VI}, and GPP_{GR}) in the non-drought years at the three flux tower sites: The VPM (a. US-Bo1, b. US-Ne1, and c. US-ARb), the TG model (d. US-Bo1, e. US-Ne1, and f. US-ARb), the VI model (g. US-Bo1, h. US-Ne1, and i. US-ARb), and the GR model (j. US-Bo1, k. US-Ne1, and l. US-ARb).

Table 5
The Pearson's correlation coefficients (r), RMSEs (g C m^{-2} day^{-1}) between flux tower-based GPP estimates (GPP_{EC}) and predicted GPP from the four EVI-based models within plant growing season in non-drought years (ND) and drought years (D) at the three flux tower sites. All correlations are significant at the 0.01 level.

Site	Status	Year	r				RMSE			
			VPM	TG	VI	GR	VPM	TG	VI	GR
US-Bo1	D	2002	0.95	0.91	0.91	0.82	1.43	3.23	2.41	4.14
	ND	2004	0.94	0.90	0.93	0.96	2.81	2.70	2.60	2.15
	ND	2006	0.98	0.95	0.94	0.97	0.93	2.86	2.01	1.94
US-Ne1	ND	2007	0.96	0.84	0.93	0.95	2.40	4.61	3.25	3.70
	ND	2008	0.97	0.96	0.96	0.95	1.87	2.63	2.54	2.83
	ND	2009	0.97	0.97	0.97	0.98	2.13	2.24	2.89	2.33
	ND	2010	0.96	0.95	0.98	0.95	2.55	3.52	1.83	3.66
	ND	2011	0.96	0.95	0.96	0.97	2.41	3.35	2.58	3.58
	D	2012	0.96	0.80	0.95	0.96	2.39	5.85	3.24	3.30
US-ARb	ND	2005	0.89	0.84	0.90	0.91	1.87	2.58	1.84	2.23
	D	2006	0.96	0.51	0.90	0.87	0.99	2.52	1.39	2.23
All site-years	ND	–	0.95	0.91	0.94	0.93	2.17	3.10	2.47	2.85
	D	–	0.97	0.83	0.94	0.94	1.61	3.90	2.32	3.16

consistent (deviation ranged from −17% to 17%) with GPP_{EC} (Table 6). In the drought site–years, however, the seasonally integrated GPP showed remarkable divergences among the four models. For example, at the US-Bo1 site in 2002, the seasonally integrated GPP estimates were 660 g C m^{-2} (GPP_{EC}), 706 g C m^{-2} (VPM), 839 C m^{-2} (TG), 982 C m^{-2} (VI), and 1062 g C m^{-2} (GR) (Table 6). At the US-Ne1 site in 2012, the seasonally integrated GPP_{EC} was 1661 g C m^{-2}, which was close to the non-drought year due to the irrigation. The estimated GPP from VPM was 1725 g C m^{-2} (4% overestimate) in 2012, but TG and VI models underestimated GPP by 12% to 20%. At the US-ARb site, in comparison with the seasonal sum of GPP_{EC} (733.6 g C m^{-2}), VPM also had the closest estimate (816.96 g C m^{-2}) while the other three models had much larger overestimates (867–1059 g C m^{-2}, Table 6). In summary, the VPM model slightly overestimated the seasonal sum of GPP in the range of 4%–11% (Table 6), while the other three models either substantially overestimated the seasonal sum of GPP (TG 20%–49%, VI 18%–27%, and GR 44%–61%) under drought conditions at the US-Bo1 and US-ARb

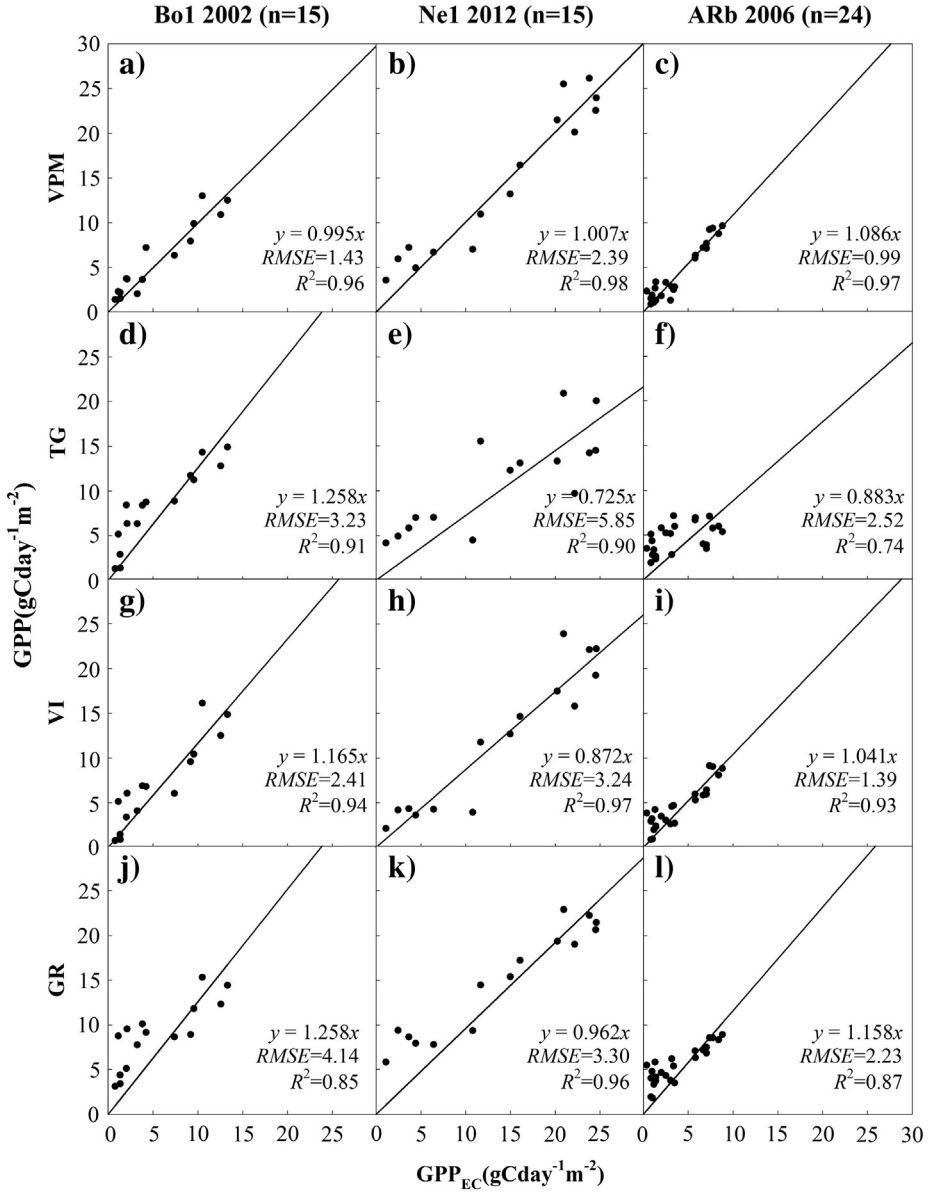

Fig. 7. The linear relationships between gross primary production from the CO2 flux tower sites (GPP_{EC}) and predicted GPP from the four models (GPP_{VPM}, GPP_{TG}, GPP_{VI}, and GPP_{GR}) in the drought years at the three flux tower sites: The VPM (a. US-Bo1, b. US-Ne1, and c. US-ARb), the TG model (d. US-Bo1, e. US-Ne1, and f. US-ARb), the VI model (g. US-Bo1, h. US-Ne1, and i. US-ARb), and the GR model (j. US-Bo1, k. US-Ne1, and l. US-ARb).

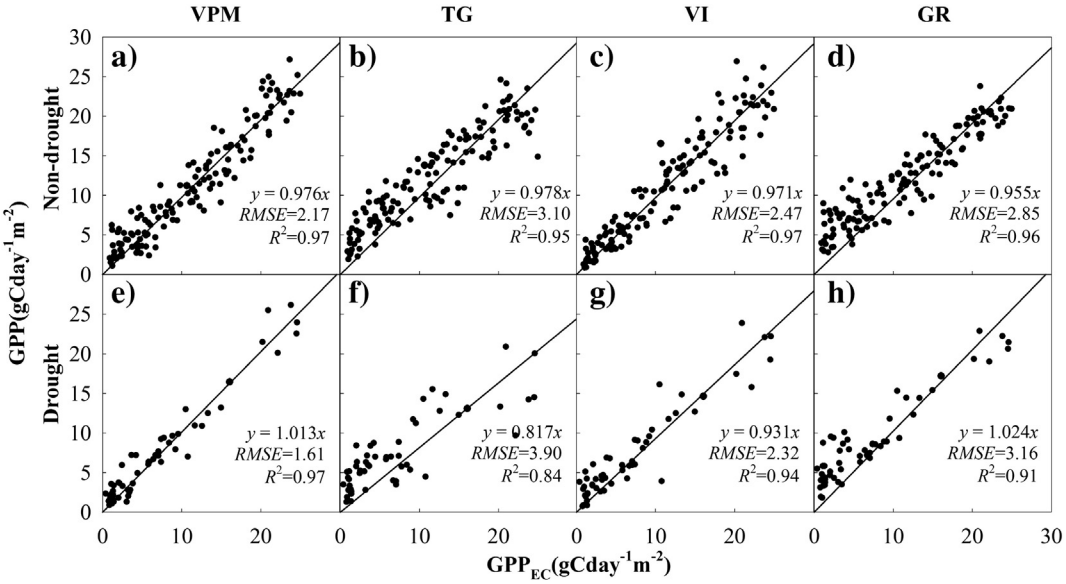

Fig. 8. The relationships between gross primary production from the CO_2 flux tower sites (GPP_{EC}) and predicted GPP from the four models in all non-drought site–years (a. GPP_{VPM}, b. GPP_{TG}, c. GPP_{VI}, and d. GPP_{GR}) and in all drought site–years (e. GPP_{VPM}, f. GPP_{TG}, g. GPP_{VI}, and h. GPP_{GR}).

sites or underestimated GPP (TG −20%, VI −12%) under drought conditions at the irrigated US-Ne1 site.

4. Discussion

4.1. Performance of EVI/FPAR$_{chl}$- and EVI/FPAR$_{green}$-based GPP models in comparison to NDVI/FPAR$_{canopy}$-based GPP models

The results from this study have shown that the predicted GPP from the four EVI-based models have good agreement with the GPP_{EC} at maize, soybean, and tallgrass prairie sites in non-drought conditions. This could be partly attributed to the application of the chlorophyll or green leaves-based theory and the use of chlorophyll-related vegetation indices (i.e., EVI) (Gitelson et al., 2014; Rossini et al., 2014). Previous study presented that EVI-based $FPAR_{chl}$ exhibited seasonal dynamics more similar with GPP_{EC} than did $FPAR_{canopy}$ from NDVI (like MOD15A2 products) (Cheng, Zhang, Lyapustin, Wang, & Middleton, 2014). In these models, EVI was used to estimate $FPAR_{chl}$, $FPAR_{green}$ and GPP. This study once again showed that the EVI has a stronger relationship with GPP than does NDVI in soybean, maize, and grassland ecosystems (Fig. 4), which is consistent with previous studies in agricultural, grassland, and forest ecosystems (Jin et al., 2013; Kalfas et al., 2011; Peng, Gitelson, & Sakamoto, 2013; Wagle et al., 2014; Wu, Niu, & Gao, 2010; Xiao, Hollinger, et al., 2004; Xiao, Zhang, et al., 2004; Xiao et al., 2005; Zhang et al., 2006).

This study focused on the inter-comparison of EVI-based models, instead of the comparison between EVI- and NDVI-based models, as previous studies have already done so (Sims et al., 2008; Sjöström et al., 2011; Wu et al., 2011). For example, the comparison of GR model and PSN model at individual sites showed that the GR model performs better in terms of model accuracy and stability (Wu, Gonsamo, Zhang, et al., 2014). In addition, VPM, TG, and VI models provided more reliable estimates of GPP than that of standard MODIS GPP products (MOD17A2), and VPM tracked well the seasonal dynamics of GPP in forests (Wu, Munger, et al., 2010). Several studies have also reported that the standard MODIS GPP products did not accurately estimate carbon uptake during drought conditions (Hwang et al., 2008; Nightingale, Coops, Waring, & Hargrove, 2007; Zhang et al., 2007). Here, we analyzed the GPP estimates from both MOD17A2 Version-5 and Version-55 for the three flux tower sites in this study (Fig. 9). The MOD17A2 products showed higher explanation of GPP variances in the non-drought years than in drought years; however, both versions of MOD17A2 products significantly underestimated GPP in both drought and non-drought years (Fig. 9).

4.2. The model structures and their sensitivities to water stress in drought years

While all the four EVI-based models in this study had good performance in the non-drought years, these models differed substantially in drought years, reflecting differences in the model design or

Table 6
The sums of gross primary production within the plant growing season (GPP, g C m^{-2}) in non-drought years (ND) and drought years (D) at the three flux tower sites. The growing season represents the period with GPP > 1 g C m^{-2} day^{-1}. The percentage numbers inside the brackets mean the overestimate or underestimate rates relative to the GPP_{EC}.

Site	Status	Year	Growing season	GPP_{EC}	GPP_{VPM}	GPP_{TG}	GPP_{VI}	GPP_{GR}
US-Bo1	D	2002	5/25–9/14	660	706 (7%)	982 (49%)	839 (27%)	1062 (61%)
	ND	2004	5/16–9/5	1198	996 (−17%)	1146 (−4%)	1241 (4%)	1289 (8%)
	ND	2006	6/2–9/14	948	906 (−4%)	1235 (30%)	1072 (13%)	1108 (17%)
US-Ne1	ND	2007	5/25–9/22	1811	1844 (2%)	1898 (5%)	1673 (−8%)	1818 (0%)
	ND	2008	6/1–10/7	1743	1697 (−3%)	1849 (6%)	1548 (−11%)	1778 (2%)
	ND	2009	5/17–9/22	1916	2015 (5%)	2097 (9%)	2096 (9%)	2070 (8%)
	ND	2010	5/25–9/6	1620	1770 (9%)	1774 (10%)	1622 (0%)	1757 (8%)
	ND	2011	6/2–10/8	1637	1644 (0%)	1763 (8%)	1538 (−6%)	1787 (9%)
	D	2012	5/16–9/5	1661	1725 (4%)	1336 (−20%)	1457 (−12%)	1772 (7%)
US-ARb	ND	2005	4/7–10/16	1513	1482 (−2%)	1490 (−2%)	1429 (−6%)	1360 (−10%)
	D	2006	4/15–10/16	734	817 (11%)	878 (20%)	866 (18%)	1059 (44%)

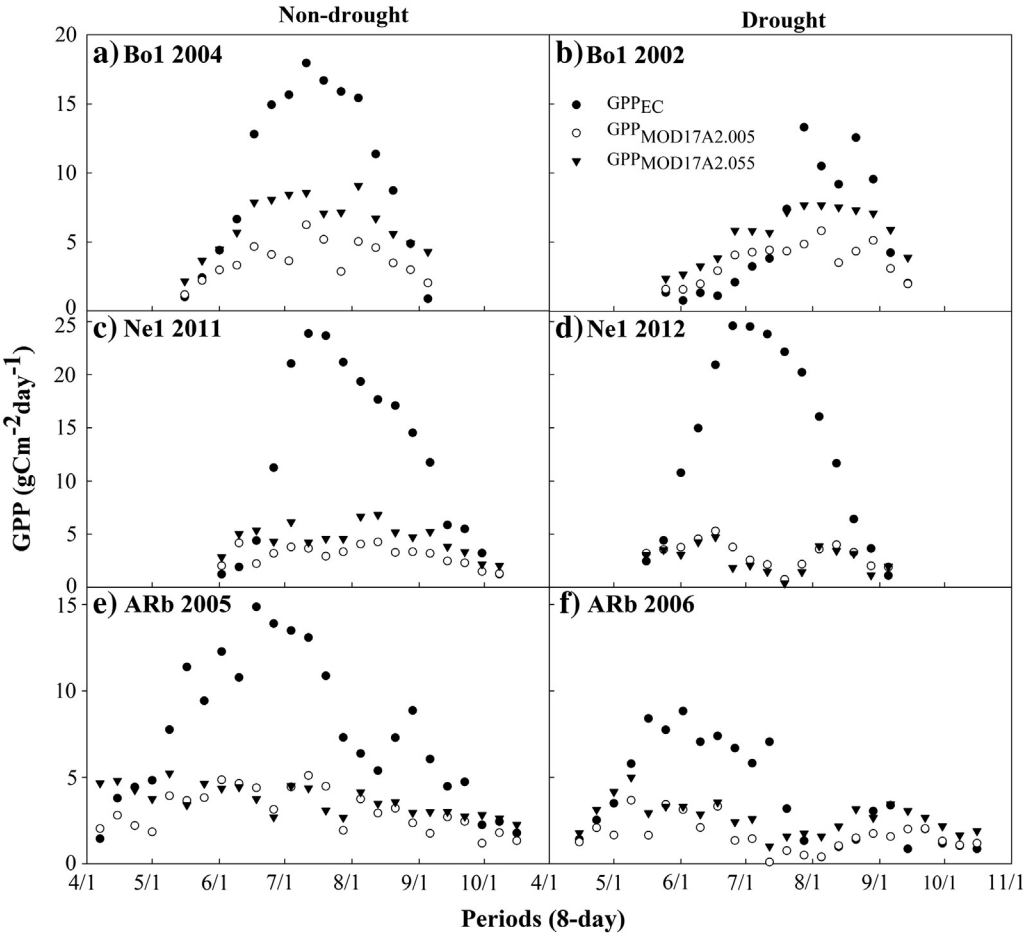

Fig. 9. The linear relationships between GPPs from the CO_2 flux tower sites (GPP_{EC}) and predicted GPP from the MOD17A2 products (including two versions of V5 and V55) in the non-drought site–years (a. US-Bo1 2004, c. US-Ne1 2011, and e. US-ARb 2005) and in the drought site–years (b. US-Bo1 2002, d. US-Ne1 2012, and f. US-ARb 2006). Like Fig. 5, only one year of data from non-drought years was used to showcase intra-annual variation of GPPs.

mechanism in addressing the effect of water stress. When drought occurs, NEE and GPP decrease considerably even from morning to afternoon hours at similar light levels because of the stomatal closure control of photosynthesis at high vapor pressure deficit (Wagle & Kakani, 2014) and low leaf and canopy water content, which is related to LSWI. It takes days to weeks for significant changes in pigment concentration and canopy structure such as shredding leaves and reduction in leaf area index, which are related to NDVI and EVI. In these four EVI-based models, the effects of droughts are represented by (1) light absorption (FPAR), (2) light use efficiency (LUE), or (3) other scalar(s) in the models. As all the four models use EVI as proxy of FPAR, the effects of drought on light absorption are considered in the same way. Thus, their differences in sensitivity to droughts are related to LUE or other scalar(s).

In the VPM, the effect of drought is considered through LUE that is down-regulated by both temperature (T_{scalar}) and water (W_{scalar}) stresses. In comparison, the other three models either have no LUE parameter (GR) or use only temperature scalar (TG) or use an alternative indicator as a proxy of LUE (VI). The GR model does not consider temperature- and water-based stress factors on LUE and GPP, and only uses chlorophyll (EVI) to estimate $FPAR_{chl}$ and GPP. Thus, it performs poorly in the drought years (Figs. 7, 8). In the VPM, LUE accounts for 67% and 78% of GPP variances in non-drought and drought years, respectively. In the VI model, LUE explains 64% of GPP variances in non-drought years but only 57% of GPP variance in drought years (57%) (Fig. 10a–f). The VI model uses EVI as a proxy for both $FPAR_{chl}$ and LUE. Our previous studies show that EVI is less sensitive to drought than LSWI and water-related variables (Wagle et al., 2014, 2015). Thus, compared to LSWI-based LUE in the VPM, EVI-based LUE in the VI model is less sensitive to droughts.

In order to compare the contributions of temperature and water scalars in the VPM model, we further decomposed the contribution of LUE into T_{scalar} and W_{scalar} by correlation analysis between GPP_{EC} and individual down-regulation scalars (Fig. 10g–j). The results show the W_{scalar} accounts for more variance of GPP than does T_{scalar} in both non-drought years (45% vs 9%, Fig. 10g, h) and drought years (28% vs 9%) (Fig. 10i, j). The low contribution of T_{scalar} to GPP variance is also consistent with the scaled LST in the TG model (Fig. 10b, e), specifically, the scaled LST accounted for 10% of GPP variance in non-drought years and <1% under drought years (Fig. 10b, e). The single air temperature or LST-based scalars cannot reflect drought effects well, as the temperature anomaly in drought years could be unremarkable (Fig. 2). Also, the scaled LST in the TG model accounts for high temperature and high VPD stress only when LST exceeds 30 °C (Sims et al., 2008), which does not occur frequently at the sites. The higher contribution of W_{scalar} in the VPM is attributed to the application of LSWI which is sensitive to water content in surface soils and vegetation (Wagle et al., 2014; Wagle et al., 2015). Also, the modified W_{scalar} function (Eq. 8) plays an important role in accounting for the effects of extreme drought on GPP. In addition to canopy-related water index (e.g., LSWI), other water-related variables have been used for assessing water stress. For example, previous study showed that drought effects on carbon uptake are more

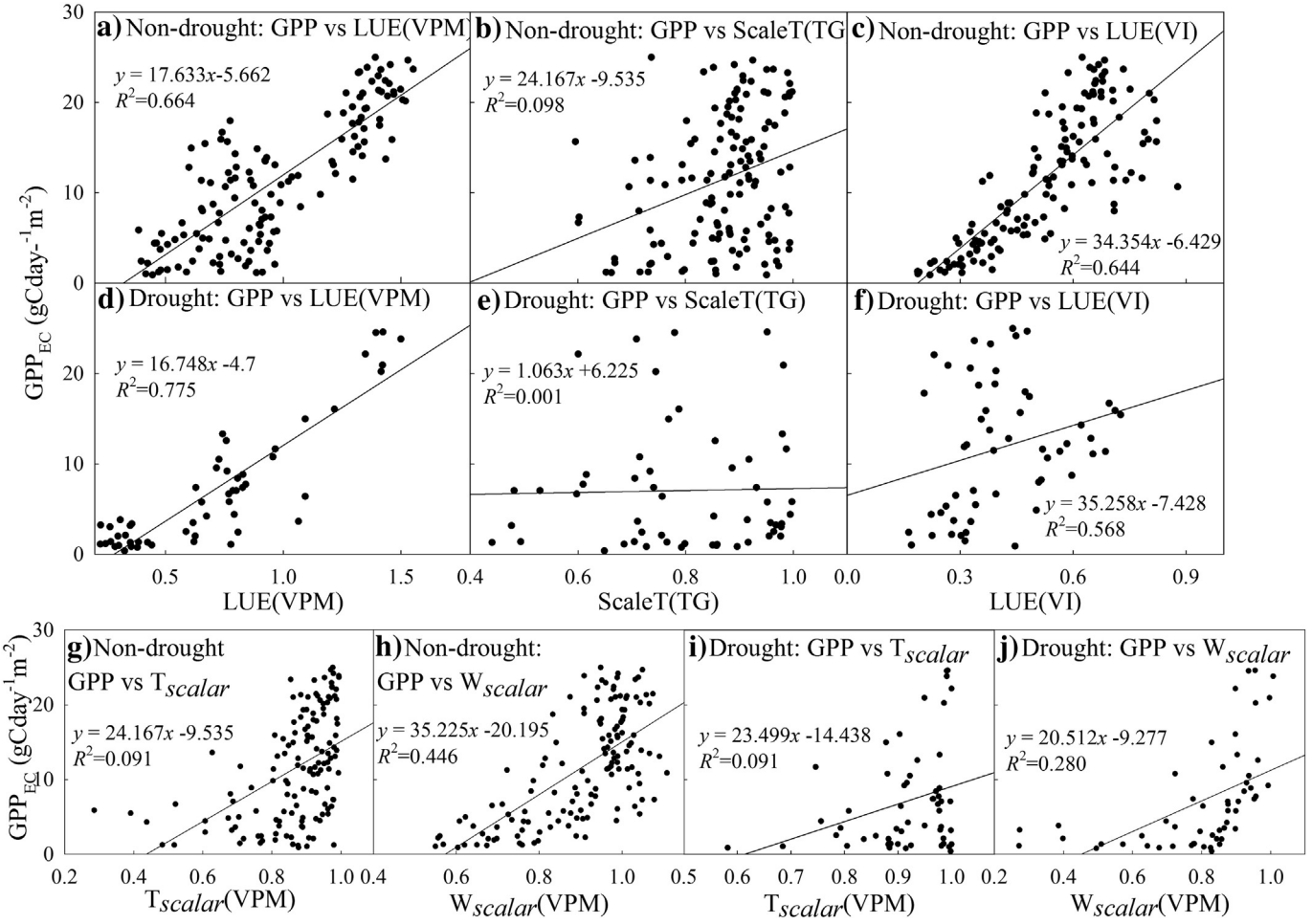

Fig. 10. The effects of light use efficiency (LUE) or environmental limitation factors of the EVI-based models on GPP in both non-drought (a. VPM, b. TG, and c. VI) and drought years (d. VPM, e. TG, and f. VI). The GR model was not included here as it does not have the LUE factor. The correlations of GPP_{EC} vs T_{scalar} and GPP_{EC} vs W_{scalar} are shown in g) and h) respectively for non-drought years, and i) and j) respectively for drought years.

closely related to soil water stress rather than atmospheric controls (temperature and VPD) (Hwang et al., 2008). However, due to spatial heterogeneity, no soil water content data are available for an ecosystem scale application.

4.3. Trade-off between comprehensiveness and applicability in satellite-based GPP models

All the four models have similar parameterization in FPAR, though the LUE estimates are different. Compared to the TG, VI, and GR models, the more sophisticated LUE structure of VPM could be the primary reason for its better performance in GPP simulations under various climate conditions. However, more parameters mean more requirements for data inputs. While the VPM can simulate GPP more accurately, TG, VI and GR models can be applied to the places without meteorological data. Model selection requires considering the ecosystem types, environmental stress status, and data availability. This study suggests that in drought areas or under drought conditions, the VPM model is a best choice among the four models. The VI model is an alternative option when no meteorological data are available. The TG and GR models can be used in the areas without water stress like irrigated croplands.

Another concern is model calibration, as the TG, VI, and GR models require calibration before application, which requires in-situ data for empirical statistical analysis. In this study, we used all the in-situ data for the model calibration (TG, VI, and GR) due to less data availability, which is not an ideal approach and can induce bias of model performance. Therefore, the actual performance of the three models could be different than what we reported here. In comparison, the VPM model only needs calibration for the maximum LUE or it can be acquired from existing publications; it is therefore more suitable to upscale simulations at various spatial and temporal domains. Satellite-derived PAR data from high spatial resolution GLASS images have been proven effective in GPP simulations (Cai et al., 2014), and the VPM model can also use LST data to replace air temperature data, which can help to reduce the dependence of the model on meteorological measurements and make VPM an independent, satellite-driven, and more operational model.

While VPM uses LSWI to determine the effect of water stress, some studies used other ancillary data or variables like LST, actual and potential evapotranspiration (AET and PET) to improve the LUE parameter (Maselli, Papale, Puletti, Chirici, & Corona, 2009; Moreno et al., 2012; Yang, Shang, Guan, & Jiang, 2013). The use of LSWI is convenient as the data are available from MODIS and Landsat. All the comparisons conducted in this study are based on the limited flux towers of crops and grasslands, and both plant types are herbaceous which have lower tolerance capability to drought, compared to woody forests (Baldocchi, Xu, & Kiang, 2004). Therefore, further evaluation of LSWI performance in drought conditions and its improvement of the water-related downscaling regulation parameter (W_{scalar}) are still needed for other ecosystem types (e.g., forest) in the future study.

5. Conclusions

In this study, we investigated and evaluated the performance and robustness of four widely used EVI-based GPP models (VPM, TG, VI, and GR) under drought conditions by using observation data from three AmeriFlux sites (soybean, grassland, and maize). Correlation analysis between GPP_{EC} and vegetation indices (NDVI and EVI) indicated that EVI and NDVI accounted for more GPP variance in drought conditions than in non-drought conditions. Furthermore, EVI accounted for more GPP variance than did NDVI in drought conditions. All the GPP estimates from the four models had generally good agreement with GPP estimates (GPP_{EC}) from the flux towers in non-drought conditions. However, their performances varied in drought conditions, and VPM was more robust during drought years than the VI, TG, and GR models. This discrepancy could be related to the inclusion of a water stress scalar in VPM based on LSWI, whereas the other three models either do not have a direct water stress scalar (GR model) or use substitutive variables (TG and VI models). This study implies that water stress regulation on light use efficiency and GPP should be considered in these models applied under drought conditions in order to estimate terrestrial carbon fluxes in the context of global climate change as well as increasing climate variability and extreme events. However, more investigations are needed to explore the possible different sensitivities of the models in the other plant function types (e.g., forests).

Acknowledgments

This study was supported in part by a research grant (Project No. 2012-02355) through the USDA National Institute for Food and Agriculture (NIFA)'s Agriculture and Food Research Initiative (AFRI), Regional Approaches for Adaptation to and Mitigation of Climate Variability and Change, and a research grant from the National Science Foundation EPSCoR (IIA-1301789). The studied AmeriFlux sites were supported by the U.S. Department of Energy (DOE), Office of Science, Office of Biological and Environmental Research (Grants No. DE-AC02-05CH11231, DE-FG03-00ER62996, DE-FG02-03ER63639, and DE-EE0003149), DOE-EPSCoR (Grant No. DE-FG02-00ER45827), and NASA NACP (Grant No. NNX08AI75G). We thank Drs. Qingyuan Zhang, Jianyang Xia, Mr. Yao Zhang and two anonymous reviewers for their comments and suggestions on the previous version of the manuscript.

References

Agarwal, D. A., Humphrey, M., Beekwilder, N. F., Jackson, K. R., Goode, M. M., & van Ingen, C. (2010). A data-centered collaboration portal to support global carbon-flux analysis. *Concurrency and Computation: Practice and Experience*, *22*, 2323–2334.

Asaf, D., Rotenberg, E., Tatarinov, F., Dicken, U., Montzka, S. A., & Yakir, D. (2013). Ecosystem photosynthesis inferred from measurements of carbonyl sulphide flux. *Nature Geoscience*, *6*, 186–190.

Baldocchi, D. (2014). Measuring fluxes of trace gases and energy between ecosystems and the atmosphere—The state and future of the eddy covariance method. *Global Change Biology*, *20*, 3600–3609.

Baldocchi, D. D., Xu, L. K., & Kiang, N. (2004). How plant functional-type, weather, seasonal drought, and soil physical properties alter water and energy fluxes of an oak-grass savanna and an annual grassland. *Agricultural and Forest Meteorology*, *123*, 13–39.

Barman, R., Jain, A. K., & Liang, M. L. (2014). Climate-driven uncertainties in modeling terrestrial gross primary production: A site level to global-scale analysis. *Global Change Biology*, *20*, 1394–1411.

Beer, C., Reichstein, M., Tomelleri, E., Ciais, P., Jung, M., Carvalhais, N., et al. (2010). Terrestrial gross carbon dioxide uptake: Global distribution and covariation with climate. *Science*, *329*, 834–838.

Cai, W. W., Yuan, W. P., Liang, S. L., Zhang, X. T., Dong, W. J., Xia, J. Z., et al. (2014). Improved estimations of gross primary production using satellite-derived photosynthetically active radiation. *Journal of Geophysical Research — Biogeosciences*, *119*, 110–123.

Cheng, Y. B., Zhang, Q. Y., Lyapustin, A. I., Wang, Y. J., & Middleton, E. M. (2014). Impacts of light use efficiency and fPAR parameterization on gross primary production modeling. *Agricultural and Forest Meteorology*, *189*, 187–197.

Desai, A. R., Richardson, A. D., Moffat, A. M., Kattge, J., Hollinger, D. Y., Barr, A., et al. (2008). Cross-site evaluation of eddy covariance GPP and RE decomposition techniques. *Agricultural and Forest Meteorology*, *148*, 821–838.

Fischer, M. L., Torn, M. S., Billesbach, D. P., Doyle, G., Northup, B., & Biraud, S. C. (2012). Carbon, water, and heat flux responses to experimental burning and drought in a tallgrass prairie. *Agricultural and Forest Meteorology*, *166*, 169–174.

Gitelson, A. A., Peng, Y., Arkebauer, T. J., & Schepers, J. (2014). Relationships between gross primary production, green LAI, and canopy chlorophyll content in maize: Implications for remote sensing of primary production. *Remote Sensing of Environment*, *144*, 65–72.

Gitelson, A. A., Vina, A., Ciganda, V., Rundquist, D. C., & Arkebauer, T. J. (2005). Remote estimation of canopy chlorophyll content in crops. *Geophysical Research Letters*, *32*.

Gitelson, A. A., Vina, A., Verma, S. B., Rundquist, D. C., Arkebauer, T. J., Keydan, G., et al. (2006). Relationship between gross primary production and chlorophyll content in crops: Implications for the synoptic monitoring of vegetation productivity. *Journal of Geophysical Research-Atmospheres*, *111*.

Goulden, M. L., Daube, B. C., Fan, S. M., Sutton, D. J., Bazzaz, A., Munger, J. W., et al. (1997). Physiological responses of a black spruce forest to weather. *Journal of Geophysical Research-Atmospheres*, *102*, 28987–28996.

Huete, A., Didan, K., Miura, T., Rodriguez, E. P., Gao, X., & Ferreira, L. G. (2002). Overview of the radiometric and biophysical performance of the MODIS vegetation indices. *Remote Sensing of Environment*, *83*, 195–213.

Huete, A. R., Liu, H. Q., Batchily, K., & vanLeeuwen, W. (1997). A comparison of vegetation indices over a global set of TM images for EOS-MODIS. *Remote Sensing of Environment*, *59*, 440–451.

Hwang, T., Kangw, S., Kim, J., Kim, Y., Lee, D., & Band, L. (2008). Evaluating drought effect on MODIS gross primary production (GPP) with an eco-hydrological model in the mountainous forest, East Asia. *Global Change Biology*, *14*, 1037–1056.

Jin, C., Xiao, X. M., Merbold, L., Arneth, A., Veenendaal, E., & Kutsch, W. L. (2013). Phenology and gross primary production of two dominant savanna woodland ecosystems in Southern Africa. *Remote Sensing of Environment*, *135*, 189–201.

Kalfas, J. L., Xiao, X., Vanegas, D. X., Verma, S. B., & Suyker, A. E. (2011). Modeling gross primary production of irrigated and rain-fed maize using MODIS imagery and CO2 flux tower data. *Agricultural and Forest Meteorology*, *151*, 1514–1528.

Maselli, F., Papale, D., Puletti, N., Chirici, G., & Corona, P. (2009). Combining remote sensing and ancillary data to monitor the gross productivity of water-limited forest ecosystems. *Remote Sensing of Environment*, *113*, 657–667.

Meijering, E. (2002). A chronology of interpolation: From ancient astronomy to modern signal and image processing. *Proceedings of the IEEE*, *90*, 319–342.

Meyers, T. P., & Hollinger, S. E. (2004). An assessment of storage terms in the surface energy balance of maize and soybean. *Agricultural and Forest Meteorology*, *125*, 105–115.

Monteith, J. L. (1972). Solar radiation and productivity in tropical ecosystems. *Journal of Applied Ecology*, *9*, 747–766.

Monteith, J. L. (1977). Climate and efficiency of crop production in Britain. *Philosophical Transactions of the Royal Society of London. Series B: Biological Sciences*, *281*, 277–294.

Moreno, A., Maselli, F., Gilabert, M. A., Chiesi, M., Martinez, B., & Seufert, G. (2012). Assessment of MODIS imagery to track light-use efficiency in a water-limited Mediterranean pine forest. *Remote Sensing of Environment*, *123*, 359–367.

Mu, Q. Z., Zhao, M. S., Heinsch, F. A., Liu, M. L., Tian, H. Q., & Running, S. W. (2007). Evaluating water stress controls on primary production in biogeochemical and remote sensing based models. *Journal of Geophysical Research — Biogeosciences*, *112*.

Nightingale, J. M., Coops, N. C., Waring, R. H., & Hargrove, W. W. (2007). Comparison of MODIS gross primary production estimates for forests across the USA with those generated by a simple process model, 3-PGS. *Remote Sensing of Environment*, *109*, 500–509.

Papale, D., Reichstein, M., Aubinet, M., Canfora, E., Bernhofer, C., Kutsch, W., et al. (2006). Towards a standardized processing of net ecosystem exchange measured with eddy covariance technique: algorithms and uncertainty estimation. *Biogeosciences*, *3*, 571–583.

Peng, Y., Gitelson, A. A., Keydan, G., Rundquist, D. C., & Moses, W. (2011). Remote estimation of gross primary production in maize and support for a new paradigm based on total crop chlorophyll content. *Remote Sensing of Environment*, *115*, 978–989.

Peng, Y., Gitelson, A. A., & Sakamoto, T. (2013). Remote estimation of gross primary productivity in crops using MODIS 250 m data. *Remote Sensing of Environment*, *128*, 186–196.

Potter, C. S. (1999). Terrestrial biomass and the effects of deforestation on the global carbon cycle — Results from a model of primary production using satellite observations. *Bioscience*, *49*, 769–778.

Potter, C. S., Randerson, J. T., Field, C. B., Matson, P. A., Vitousek, P. M., Mooney, H. A., et al. (1993). Terrestrial ecosystem production — A process model-based on global satellite and surface data. *Global Biogeochemical Cycles*, *7*, 811–841.

Prince, S. D. a. S. J. G. (1995). Global primary production: A remote sensing approach. *Journal of Biogeography*, *22*, 316–336.

Raich, J., Rastetter, E., Melillo, J., Kicklighter, D., Steudler, P., Peterson, B., et al. (1991). Potential net primary productivity in South America: Application of a global model. *Ecological Applications*, *1*, 399–429.

Reichstein, M., Falge, E., Baldocchi, D., Papale, D., Aubinet, M., Berbigier, P., et al. (2005). On the separation of net ecosystem exchange into assimilation and ecosystem respiration: Review and improved algorithm. *Global Change Biology*, *11*, 1424–1439.

Rossini, M., Migliavacca, M., Galvagno, M., Meroni, M., Cogliati, S., Cremonese, E., et al. (2014). Remote estimation of grassland gross primary production during extreme meteorological seasons. *International Journal of Applied Earth Observation and Geoinformation*, *29*, 1–10.

Running, S. W., Nemani, R. R., Heinsch, F. A., Zhao, M. S., Reeves, M., & Hashimoto, H. (2004). A continuous satellite-derived measure of global terrestrial primary production. *Bioscience*, *54*, 547–560.

Running, S. W., Thornton, P. E., Nemani, R., & Glassy, J. M. (2000). Global terrestrial gross and net primary productivity from the Earth Observing System. In O. E. Sala, R. B. Jackson, H. A. Mooney, & R. W. Howarth (Eds.), *Methods in ecosystem science* (pp. 44–57). New York: Springer Verlag.

Schaefer, K., Schwalm, C. R., Williams, C., Arain, M. A., Barr, A., Chen, J. M., et al. (2012). A model-data comparison of gross primary productivity: Results from the North American Carbon Program site synthesis. *Journal of Geophysical Research — Biogeosciences*, *117*.

Sims, D. A., Rahman, A. F., Cordova, V. D., El-Masri, B. Z., Baldocchi, D. D., Bolstad, P. V., et al. (2008). A new model of gross primary productivity for North American ecosystems based solely on the enhanced vegetation index and land surface temperature from MODIS. *Remote Sensing of Environment*, *112*, 1633–1646.

Sims, D. A., Rahman, A. F., Cordova, V. D., El-Masri, B. Z., Baldocchi, D. D., Flanagan, L. B., et al. (2006). On the use of MODIS EVI to assess gross primary productivity of North American ecosystems. *Journal of Geophysical Research — Biogeosciences*, *111*.

Sjöström, M., Ardö, J., Arneth, A., Boulain, N., Cappelaere, B., Eklundh, L., et al. (2011). Exploring the potential of MODIS EVI for modeling gross primary production across African ecosystems. *Remote Sensing of Environment*, *115*, 1081–1089.

Song, C. H., Dannenberg, M. P., & Hwang, T. (2013). Optical remote sensing of terrestrial ecosystem primary productivity. *Progress in Physical Geography*, *37*, 834–854.

Suyker, A. E., Verma, S. B., Burba, G. G., & Arkebauer, T. J. (2005). Gross primary production and ecosystem respiration of irrigated maize and irrigated soybean during a growing season. *Agricultural and Forest Meteorology*, *131*, 180–190.

Tucker, C. J. (1979). Red and photographic infrared linear combinations for monitoring vegetation. *Remote Sensing of Environment*, *8*, 127–150.

Wagle, P., & Kakani, V. G. (2014). Environmental control of daytime net ecosystem exchange of carbon dioxide in switchgrass. *Agriculture, Ecosystems & Environment*, *186*, 170–177.

Wagle, P., Xiao, X., & Suyker, A. E. (2015). Estimation and analysis of gross primary production of soybean under various management practices and drought conditions. *ISPRS Journal of Photogrammetry and Remote Sensing*, *99*, 70–83.

Wagle, P., Xiao, X. M., Torn, M. S., Cook, D. R., Matamala, R., Fischer, M. L., et al. (2014). Sensitivity of vegetation indices and gross primary production of tallgrass prairie to severe drought. *Remote Sensing of Environment*, *152*, 1–14.

Wu, C., Chen, J. M., Desai, A. R., Hollinger, D. Y., Arain, M. A., Margolis, H. A., et al. (2012). Remote sensing of canopy light use efficiency in temperate and boreal forests of North America using MODIS imagery. *Remote Sensing of Environment*, *118*, 60–72.

Wu, C. Y., Chen, J. M., & Huang, N. (2011). Predicting gross primary production from the enhanced vegetation index and photosynthetically active radiation: Evaluation and calibration. *Remote Sensing of Environment*, *115*, 3424–3435.

Wu, C., Gonsamo, A., Gough, C. M., Chen, J. M., & Xu, S. (2014a). Modeling growing season phenology in North American forests using seasonal mean vegetation indices from MODIS. *Remote Sensing of Environment*, *147*, 79–88.

Wu, C. Y., Gonsamo, A., Zhang, F. M., & Chen, J. M. (2014b). The potential of the greenness and radiation (GR) model to interpret 8-day gross primary production of vegetation. *ISPRS Journal of Photogrammetry and Remote Sensing*, *88*, 69–79.

Wu, C. Y., Munger, J. W., Niu, Z., & Kuang, D. (2010a). Comparison of multiple models for estimating gross primary production using MODIS and eddy covariance data in Harvard Forest. *Remote Sensing of Environment*, *114*, 2925–2939.

Wu, C. Y., Niu, Z., & Gao, S. A. (2010b). Gross primary production estimation from MODIS data with vegetation index and photosynthetically active radiation in maize. *Journal of Geophysical Research-Atmospheres*, *115*.

Wu, C. Y., Niu, Z., Tang, Q., Huang, W. J., Rivard, B., & Feng, J. L. (2009). Remote estimation of gross primary production in wheat using chlorophyll-related vegetation indices. *Agricultural and Forest Meteorology*, *149*, 1015–1021.

Wu, C. Y., Niu, Z., Wang, J. D., Gao, S. A., & Huang, W. J. (2010c). Predicting leaf area index in wheat using angular vegetation indices derived from in situ canopy measurements. *Canadian Journal of Remote Sensing*, *36*, 301–312.

Xiao, X., Hollinger, D., Aber, J., Goltz, M., Davidson, E. A., Zhang, Q., et al. (2004a). Satellite-based modeling of gross primary production in an evergreen needleleaf forest. *Remote Sensing of Environment*, *89*, 519–534.

Xiao, X. M., Zhang, Q. Y., Braswell, B., Urbanski, S., Boles, S., Wofsy, S., et al. (2004b). Modeling gross primary production of temperate deciduous broadleaf forest using satellite images and climate data. *Remote Sensing of Environment*, *91*, 256–270.

Xiao, X. M., Zhang, Q. Y., Hollinger, D., Aber, J., & Moore, B. (2005). Modeling gross primary production of an evergreen needleleaf forest using MODIS and climate data. *Ecological Applications*, *15*, 954–969.

Yang, Y. T., Shang, S. H., Guan, H. D., & Jiang, L. (2013). A novel algorithm to assess gross primary production for terrestrial ecosystems from MODIS imagery. *Journal of Geophysical Research — Biogeosciences*, *118*, 590–605.

Yuan, W. P., Liu, S., Zhou, G. S., Zhou, G. Y., Tieszen, L. L., Baldocchi, D., et al. (2007). Deriving a light use efficiency model from eddy covariance flux data for predicting daily gross primary production across biomes. *Agricultural and Forest Meteorology*, *143*, 189–207.

Zhang, Q. Y., Middleton, E. M., Cheng, Y. B., & Landis, D. R. (2013). Variations of foliage chlorophyll fAPAR and foliage non-chlorophyll fAPAR (fAPAR(chl), fAPAR(non-chl)) at the Harvard Forest. *IEEE Journal of Selected Topics in Applied Earth Observations and Remote Sensing*, *6*, 2254–2264.

Zhang, Q. Y., Middleton, E. M., Margolis, H. A., Drolet, G. G., Barr, A. A., & Black, T. A. (2009). Can a satellite-derived estimate of the fraction of PAR absorbed by chlorophyll (FAPAR(chl)) improve predictions of light-use efficiency and ecosystem photosynthesis for a boreal aspen forest? *Remote Sensing of Environment*, *113*, 880–888.

Zhang, L., Wylie, B., Loveland, T., Fosnight, E., Tieszen, L. L., Ji, L., et al. (2007). Evaluation and comparison of gross primary production estimates for the Northern Great Plains grasslands. *Remote Sensing of Environment*, *106*, 173–189.

Zhang, Q. Y., Xiao, X. M., Braswell, B., Linder, E., Ollinger, S., Smith, M. L., et al. (2006). Characterization of seasonal variation of forest canopy in a temperate deciduous broadleaf forest, using daily MODIS data. *Remote Sensing of Environment*, *105*, 189–203.

Zhao, M. S., Heinsch, F. A., Nemani, R. R., & Running, S. W. (2005). Improvements of the MODIS terrestrial gross and net primary production global data set. *Remote Sensing of Environment*, *95*, 164–176.

Zhao, M. S., & Running, S. W. (2010). Drought-induced reduction in global terrestrial net primary production from 2000 through 2009. *Science*, *329*, 940–943.

Zscheischler, J., Mahecha, M. D., von Buttlar, J., Harmeling, S., Jung, M., Rammig, A., et al. (2014). A few extreme events dominate global interannual variability in gross primary production. *Environmental Research Letters*, *9*.